Int J Earth Sci (Geol Rundsch) (2008) 97:205–226
DOI 10.1007/s00531-007-0254-3

ORIGINAL PAPER

Spherical harmonic analysis of earth's conductive heat flow

V. M. Hamza · R. R. Cardoso · C. F. Ponte Neto

Received: 9 February 2007 / Accepted: 12 September 2007 / Published online: 17 October 2007

Abstract A reappraisal of the international heat flow database has been carried out and the corrected data set was employed in spherical harmonic analysis of the conductive component of global heat flow. Procedures used prior to harmonic analysis include analysis of the heat flow data and determination of representative mean values for a set of discretized area elements of the surface of the earth. Estimated heat flow values were assigned to area elements for which experimental data are not available. However, no corrections were made to account for the hypothetical effects of regional-scale convection heat transfer in areas of oceanic crust. New sets of coefficients for 12° spherical harmonic expansion were calculated on the basis of the revised and homogenized data set. Maps derived on the basis of these coefficients reveal several new features in the global heat flow distribution. The magnitudes of heat flow anomalies of the ocean ridge segments are found to have mean values of less than 150 mW/m^2. Also, the mean global heat flow values for the raw and binned data are found to fall in the range of 56–67 mW/m^2, down by nearly 25% compared to the previous estimate of 1993, but similar to earlier assessments based on raw data alone. To improve the spatial resolution of the heat flow anomalies, the spherical harmonic expansions have been extended to higher degrees. Maps derived using coefficients for 36° harmonic expansion have allowed identification of new features in regional heat flow fields of several oceanic and continental segments. For example, lateral extensions of heat flow anomalies of active spreading centers have been outlined with better resolution than was possible in earlier studies. Also, the characteristics of heat flow variations in oceanic crust away from ridge systems are found to be typical of conductive cooling of the lithosphere, there being little need to invoke the hypothesis of unconfined hydrothermal circulation on regional scales. Calculations of global conductive heat loss, compatible with the observational data set, are found to fall in the range of 29–34 TW, nearly 25% less than the 1993 estimate, which rely on one-dimensional conductive cooling models.

Keywords Global heat flow · Spherical harmonic analysis · Conduction heat transfer

Introduction

Since the pioneering work by Everett (1883), several attempts have been made to estimate mean heat flow of the earth, based on results of experimental heat flow measurements. These include, among others, the works of Birch (1954), Lee and Uyeda (1965), Horai and Simmons (1969), Chapman and Pollack (1975) and Jessop et al. (1976). Since the decade of 1970 significant progress has been achieved in data acquisition, with direct determination of heat flow in several major tectonic regions of the earth. However, the improvements in the global data base have not lead to substantial changes in these earlier estimates. Nevertheless, in presenting the updated compilation of global heat flow data, Pollack et al. (1993) arrived at an estimate of 87 mW/m^2 for the mean heat flow of the earth, which is nearly 30% higher than the previous ones. An examination of their procedure reveals that the estimate of high mean heat flow is not based on experimental data, but a consequence of the large-scale use of theoretical values for large segments of the young oceanic crust. Pollack et

V. M. Hamza (✉) · R. R. Cardoso · C. F. Ponte Neto
Observatório Nacional, Rua General José Cristino, 77,
Rio de Janeiro, Brazil
e-mail: hamza@on.br

al. (1993) justify this procedure on the ground that experimental heat flow values for the ocean crust do not account for heat transfer by hydrothermal activity and hence are not representative of the total heat flux. The implicit assumption behind this argument is that active unconfined hydrothermal systems operate on regional scales in large parts of the oceanic crust, and that a one-dimensional conductive cooling model correctly account for the difference.

In our understanding the hypothesis of unconfined hydrothermal circulation (which is the basis for the use of theoretical heat flow values) is questionable in the light of available information on the thermal and hydrological characteristics of the ocean crust. The relevant information may be summarized as follows:

1. The presence of hydrothermal convection in deeper layers of the oceanic crust need not necessarily lead to systematic errors in conductive heat flow values. In much of the ocean crust the upper layer of basaltic rocks, where fluid circulation is believed to take place, is overlain by low permeability sediments. Under such conditions, the sedimentary layer act as a confining lid on underlying hydrothermal circulation systems. Measurements of conductive heat transfer in such confining layers are known to provide reasonable estimate of background heat flux (Garg and Kassoy 1981; Holst and Aziz 1972; Ribando and Torrance 1976). Only in areas of unconfined circulation does conduction heat transfer lead to underestimation of total heat loss (Cheng and Lau 1974; Pratts 1966);
2. Direct evidences pointing to the occurrence of heat transfer by thermal fluid discharges in the ocean floor are limited to faults and fracture zones situated in ridge crests and ridge flanks of active spreading centers (Baker et al. 1996; Embley et al. 1991; German et al. 1994; Haymon et al. 1991; Lupton et al. 1993; Murton et al. 1994; Williams et al. 1974 among others). Fluid discharges emanating from deep circulation systems are rare in areas of ocean crust away from spreading centers. It is not a ubiquitous heat transfer process operating in ocean crust blanketed by sediments;
3. Marine heat flow measurements are usually neither preceded nor accompanied by detailed mapping of local fracture zones and fluid circulation systems of the ocean floor (Lubimova et al. 1965; Jones 1999). Given the lack of knowledge of the mechanical, thermal and hydrological characteristics of underlying rock strata, it seems reasonable to assume that the sites of heat flow measurements are randomly distributed with respect to the fracture systems. In such cases, heat flow values averaged over large area elements are unlikely to lead to biased estimates;
4. The sedimentary layers in the ocean floor are characterized by relatively low permeability (10^{-18}–10^{-14} m^2/s), which is several orders of magnitude less than the permeability of fracture zones in basalts (Becker and Davis 2003; Becker and Fisher 2000; Bryant et al. 1981; Fisher 1998; Giambalvo et al. 2000; Hamilton 1976 among others). The rapidly accumulating sediment cover over the young ocean crust is known to act as an impermeable barrier against widespread occurrence of unconfined hydrothermal systems (Snelgrove and Forster 1996);
5. In fault or fracture controlled hydrothermal systems the perturbations of heat flow field are generally limited to rather narrow belts of recharge and discharge zones (Goyal and Kassoy 1977; Gray et al. 1976 among others). The lateral dimensions of unperturbed areas lying between these zones are several orders of magnitude larger than those of fracture zones themselves (Alexandrino and Hamza 2005; Turcotte and Schubert 1982). Hence the probability that measurement sites are preferentially situated on or close to recharge zones of hydrothermal systems is relatively small. Randomly distributed measurements are unlikely to provide biased estimates of background heat flow;
6. Because of complexities in deep-sea operations and limitations of experimental techniques most of the oceanic heat flow measurements are carried out at sites where sedimentary cover is present (Jones 1999). In such areas the heat flow field is most likely unperturbed;
7. Chemical reactions and mineral precipitations lead to drastic reductions in permeability of the circulation systems over time-scales relatively short compared with the age of the oceanic lithosphere (Akaku 1988; Drummond and Ohmoto 1985; Lowell et al. 1993; Meyer and Hemley 1967). Under such conditions it is reasonable to assume that the permeability of fracture systems falls off rapidly with distance from the ridge areas. This appears to be a major limiting factor that inhibit occurrence of large-scale convective movements in the old ocean crust; and
8. The convection systems proposed for the ocean crust away from ridge zones have upwelling limbs situated in the relatively colder parts of the lithosphere and down-going limbs situated within the warmer parts. Such a situation is contrary to what is normally observed in natural thermal convection systems (Cheng 1978; Combarnous and Bories 1975; Elder 1981).

Other relevant factors to be considered in this context are the geochemical constraints on overall heat loss of the earth. As noted by Hofmeister and Criss (2005) these constraints lead to estimates that differ significantly from that of Pollack et al. (1993). Also, the comments by Von Herzen et al. (2005) on the recent work of Hofmeister and Criss (2005) and that by Hofmeister and Criss (2006) on the work of Wei and Sandwell (2006) indicate that there are considerable disagreements in the current assessments of global heat flow. Also, the parameters used by Pollack et al. (1993) are not appropriate, as shown by recent measurements of thermal conductivities. In this context, reexaminations of the primary geothermal data base and the procedures used in harmonic representations of global heat flow are in order.

The present work reports results of harmonic analysis of the revised global heat flow database, following a procedure that makes full use of the entire observational data set. Initially, a reassessment of the global heat flow database is carried out, based on the recent works of Ponte Neto and Hamza (2004), Cardoso et al. (2005) and Cardoso and Hamza (2006). The corrected data base is subsequently used in determining representative mean heat flow values for a regular grid system composed of $5° \times 5°$ area elements of the surface of the earth. Because the emphasis of the present work is in investigating conductive heat flow variations, we refrained from the practice of using theoretical heat flow values as a substitute for experimental data. The regularized data set is used to calculate new sets of harmonic coefficients and in deriving new global heat flow maps.

Reappraisal of the IHFC database

The global heat flow database in its present form is an outgrowth of earlier compilations by Birch (1954), Lee (1963), Lee and Uyeda (1965), Jessop et al. (1976) and Pollack et al. (1993). Progress in data acquisition during the decades prior to 1980 has not only lead to substantial improvements in outlining regional heat flow anomalies but also better representations of the global thermal field. Since 1990 however, advances in data acquisition has been relatively slow, being restricted mainly to areas of low data density in the Asian and South American continents.

The database available for download at the web site of NGDC includes 21,453 records of heat flow measurements over the globe. Of these 12,105 are on land, 9,053 in oceanic regions, and the remaining 295 in transition regions, such as continental platform areas and shallow water bodies. The format adopted for the individual fields of information has been discussed in detail by Balling et al. (1981), but the data set as a whole remains essentially as an intercalating system of tables and references. Only recently has steps been taken to implement spreadsheet based systems, suitable for automatic processing (Gosnold, personal communication).

The database may be considered as composed of essentially three parts: continental, oceanic, and transition regions. These are further subdivided into several subsets. Regarding continental areas, the data for the different countries are grouped into separate tables. For oceanic regions several sets of data have been put together, following roughly the chronological order of heat flow measurements. Consequently, careful and detailed preprocessing is necessary for extracting data sets for the different tectonic units. Also, classification of data sets for continental platform areas, inland seas and water bodies do not appear to follow any consistent or systematic schemes. Such difficulties are probably the main underlying reason for the very few attempts, which have so far been made, in examining heat flow variations on a global scale.

The distribution of heat flow data over the globe is illustrated in Fig. 1. Recent compilations reported by Hamza and Muñoz (1996) and Hamza et al. (2005) were also included to improve the regional distribution for the South American continent. It is clear to note that the availability of data is reasonable in several of the major regional sectors and geotectonic units in both continental and oceanic regions. However, areas of poor data density exist in continental areas of North Africa, Central Asia, and South America, as well as in Polar regions of the northern and southern hemispheres. High latitude areas of southern oceans also have poor data coverage.

In carrying out a reappraisal of the IHFC database, it was considered important to check the internal consistency of the database. This, however, turned out to be a task that could not easily be automated, in view of the archaic structure of the database. To circumvent this problem a spread sheet based system was implemented, which allowed verification of the individual data fields. Detailed verification revealed widespread occurrence of transcription and/or typographic errors in the database, unnoticed in earlier studies. The verification also revealed that the

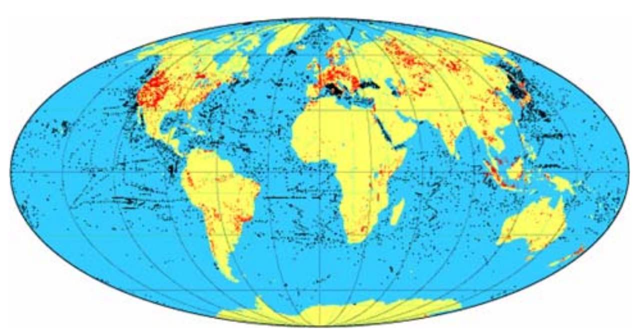

Fig. 1 Global distribution of heat flow data. The *black dots* indicate locations of measurements in oceanic areas whereas *red dots* indicate that in continental areas

classification systems adopted for data from continental platform areas, inland seas and water bodies do not follow a consistent pattern. Also, there are cases where heat flow data obtained as part of projects that span over more than one country are simply listed as belonging to the country of the principal investigator. Such problems have lead to some degree of confusion in analysis and interpretation of the data. As an illustrative example, consider the data set for Switzerland, which lists heat flow measurements for 104 localities. Only 78 of these are located within the country limits of Switzerland, the remaining ones are found to be in neighboring areas of France, Italy and Germany. Similar problems exist with data sets for many other countries in the continents of Asia, Africa, and North America.

Clearly, there is a need for restructuring and reformatting the database. Recently, Cardoso et al. (2005) and Cardoso (2006) have proposed corrections for the occurrence of what they call as "large-scale" errors in the coordinates. Table 1 provides a summary list of such corrections in the coordinates. Most of the corrections are for continental areas of Asia, Europe, and North America. A number of incorrect locations were also found for data from oceanic regions. No corrections were found necessary for the more recent data from South America and the Antarctic.

Previous representations of global heat flow

Early attempts for harmonic analyses of heat flow data were carried out by Lee and MacDonald (1963), Lee and Uyeda (1965) and Horai and Simmons (1969). The procedures employed in these early works rely on analytical methods that generate an over-determined set of equations based on experimental data, which in turn is solved for the unknown coefficients. This approach has the inherent weakness that the harmonic representations in areas devoid

Table 1 Summary list of corrections for the IHFC database

Region	Number of data		Total
	Correct locations	Incorrect locations	
Africa	526	21	547
Central America	83	1	84
South America	822	0	822
Antarctic	9	0	9
Asia	3,967	365	4,332
Europe	1,943	112	2,055
North America	4,466	156	4,622
Australia and Pacific	264	23	287
Seas and Oceans	9,179	169	9,348
Total	2,1259	847	2,2106

of data are sensitive to numerical instabilities. In such cases, the values of the harmonic coefficients depend to a large extent on the data density and also characteristics of the data distribution.

In the work of Chapman and Pollack (1975), hereafter abbreviated as C&P, problems arising from uneven data distribution are minimized by employing discretized data sets and using estimated values for grid elements for which experimental data are not available. The estimates are based on the empirical heat flow-age relations proposed by Polyak and Smirnov (1968) and Hamza and Verma (1969). The use of empirical relations has the advantage that it allows better control on numerical instabilities in harmonic representation. In the work of C&P, mean heat flow were calculated for $5° \times 5°$ area elements which were subsequently employed in calculating the Legendre coefficients of the spherical harmonic expansion. Two sets of coefficients were calculated: one based exclusively on estimated values for all the grid elements and a second one in which use of estimated values is limited to grid elements devoid of experimental data. The global heat flow maps presented by C&P are derived from these two sets of harmonic coefficients. However, harmonic expansion was carried out only up to degree 12. Hence, the maps derived by C&P display mainly large scale variations in the global conductive heat flow. It also lacks the spatial resolution needed for identifying thermal features associated with local tectonic units.

In spite of such limitations, the maps derived by C&P revealed several important characteristics of global heat flow distribution. Prominent among these are the heat flow anomalies located along the East pacific and South India Ocean ridge systems. High heat flow also occurs along the back-arc regions of the west Pacific and also along the mid-ocean ridge systems. In addition, small scale heat flow anomalies have been identified in the Red Sea area and also in the Persian Gulf and in the Gulf of California. On the other hand, the continents of Asia, Europe, Africa, North America, South America and Australia are identified as areas with heat flux less than 50 mW/m^2. According to the harmonic analysis of C&P, the mean heat flux of the earth is 59 mW/m^2.

The work of Pollack et al. (1993), hereafter abbreviated as PH&J, is based largely on the now updated compilation consisting of experimental heat flow values for 20,201 localities. This data set was employed in calculating mean heat flow for a regular grid system composed of $5° \times 5°$ area elements. However, a careful examination of their procedure reveals that significant modifications were introduced in selecting heat flow values for the grid elements. For example, the use of experimental data and of the estimated values is restricted to areas of old ocean basins and continental margins. In addition, theoretical heat flow values, derived from plate cooling models (McKenzie 1967; Sclater et al. 1980; Stein and Stein 1992) were used for selected segments of ocean ridge areas. This procedure is based on the argument that experimental heat flow data fail to account for heat transfer by supposed hydrothermal circulation in the ocean crust with ages of up to 65 million years. The implicit assumption is that active unconfined hydrothermal systems operate on a regional scale in more than 70% of the oceanic crust.

In our understanding, the practice of using theoretical values as substitute for experimental data is open to criticism, as it is based on assumptions as to the nature of thermal processes at deeper levels in the crust, which is what we are trying to determine in the first place. Another problem with this procedure is that it requires extensive pre-processing of related geological and geophysical information, relevant for heat and mass transfer in a large number of marine tectonic units. In many cases, such supplementary information are not readily available. Detailed geologic mapping of basement structures that control fluid flow beneath ocean basins have not so far been carried out, for obvious limitations in current technological capabilities and because of the costs involved. As a result, the present level of knowledge about the tectonic and structural features of basement layer beneath sediments in oceanic areas is far inferior to that for the crust in continental areas. In spite of the large number of investigations carried out in deep sea areas, much less is known of the deep structure of oceanic crust than its continental counterpart.

At this point, a brief comment on the nature of data sets rejected by PH&J in their analysis of global heat flow is in order. Table 2 provides a summary of the observational data sets that were rejected for the ridge areas of southern oceans. The data have been grouped into 10° × 10° grid elements. The coordinates of these grid elements are given in columns (2) and (3), means of observed heat flow values in column (4) and number of data points in column (5). Note that the mean values of the rejected data sets for these grid elements fall in the range of 36.9–127 mW/m^2 for the South Atlantic, 30.9–97 mW/m^2 for the Indian Ocean and 18.2–328.6 mW/m^2 for the Pacific Ocean. These ranges are quite large compared with the uncertainties in oceanic heat flow measurements. It also reveals that the rejected data set includes not only relatively low values (<40 mW/m^2) but also values higher than the global average. The criteria for rejection of high heat flow values, which are usually considered as unaffected by down flow of cold fluids, was not discussed explicitly by PH&J. The total number of rejected data for the ridge segments of the southern oceans is 1669, which constitutes nearly 20% of the global ocean heat flow data set.

Table 2 Summary of the observational data sets for the southern oceans, rejected by Pollack et al. (1993)

Oceanic region	Longitude	Latitude	Mean heat flow (mW/m^2)	No. of data
Atlantic	–15	–5	53,75	42
	–15	–15	70,93	81
	–5	–15	36,92	18
	–15	–25	79,40	30
	–5	–25	44,95	14
	–15	–35	82,83	23
	–5	–35	69,65	34
	–15	–45	39,80	1
	–15	–55	46,85	2
	–5	–55	127,00	4
Indian	65	–15	41,50	25
	75	–15	53,99	17
	65	–25	86,36	29
	75	–25	82,49	15
	65	–35	43,30	13
	75	–35	47,01	7
	85	–35	67,55	4
	95	–35	30,22	4
	75	–45	49,83	6
	95	–45	64,50	1
	105	–45	95,00	1
	115	–45	35,80	2
	125	–45	37,45	2
	135	–45	54,40	1
	145	–45	97,00	9
	65	–55	63,37	3
	75	–55	55,30	1
Pacific	–115	15	117,86	24
	–105	15	125,11	45
	–95	15	55,11	57
	–115	5	75,34	66
	–105	5	88,99	27
	–95	5	35,97	26
	–85	5	328,61	776
	–115	–5	84,97	12
	–105	–5	124,23	31
	–95	–5	109,61	23
	–125	–15	49,42	22
	–115	–15	111,78	98
	–105	–15	121,45	51
	–125	–25	66,26	8
	–115	–25	167,95	4
	–105	–25	107,90	4
	–125	–45	18,25	2
	–115	–45	86,30	1
	–105	–45	107,75	2
	–95	–45	96,30	1

The data are grouped into 10° × 10° grid elements

A detailed examination of the database employed by PH&J indicates that results of experimental data were used for only 1,192 grid elements while theoretical heat flow values were used for 835 grid elements. In addition, estimated heat flow values were employed for the remaining 565 grid elements. The large number of grid elements (nearly 32% of the total data set) for which theoretical values were adopted is a characteristic feature of the data set employed by PH&J. Also, in spite of the considerable improvements in the experimental data set, PH&J limited their harmonic representation to degree 12. Hence the map derived in their studies outlines only large scale variations in global heat flow. It depicts most of the continental regions as having mean heat flux of up to 85 mW/m^2 whereas the ocean ridge systems are depicted as regions with heat flux in excess of 150 mW/m^2. Another outstanding feature in the map of PH&J is the presence of three major regions in the southern oceans, where heat flux is depicted as having values higher than 200 mW/m^2. These include ridge areas in the East Pacific, South Mid Atlantic, and South East Indian Oceans. According to the harmonic analysis of PH&J, the value of the first coefficient is 87 mW/m^2, which implies that the mean heat flow of the earth is nearly 30% higher than the previous estimates.

Though large scale heat flow variations in the global map of PH&J appear at first sight as similar to those outlined in earlier studies a closer examination reveals that significant differences exist. Figure 2 illustrates the differences between global heat flow representations of C&P and PH&J. Note that the magnitudes of heat flow anomalies in the harmonic representation of PH&J are systematically high in both continental and oceanic regions. Such differences may arise as a result of improvements in the database, or a consequence of the widespread use of theoretical heat flow values for oceanic crust. This is a matter of crucial importance in studies of the global thermal fields, but has not received due attention over the last few decades.

Harmonic analysis of conductive heat flow

The problems identified in the harmonic representations of PH&J point to the need for analysis of the global heat flow dataset without recourse to the use of theoretical values. In the present work, we make use of the revised and updated data base set up by Cardoso et al. (2005) and Cardoso (2006). The procedures employed in discretization of this data set are in many aspects similar to those employed in previous studies of C&P and PH&J. Initially mean heat flow values were calculated for $5° \times 5°$ area elements, based on the available data set. Experimental data are available for 1,239 of such grid elements, out of a total of 2,592, there being 1,353 without data. However, most of grid elements with data are situated in low latitudes and hence its total surface area is higher than that for grid elements without data. Following the procedure of C&P use is made of the empirical predictor in assigning estimated heat flow values to those grid elements for which experimental data are not yet available. The characteristics of the resultant grid system are outlined in the map of Fig. 3 where the red dots indicate area elements for which experimental data are available while the white dots indicate those for which estimated values were employed. As mentioned earlier, theoretical values derived from plate cooling models were not considered in estimating heat flow for the young ocean crust.

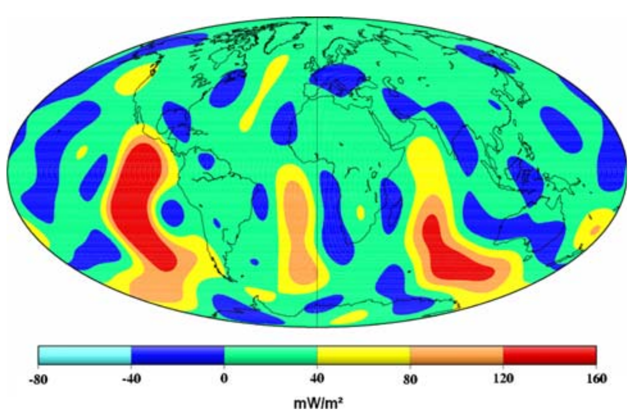

Fig. 2 Map of differences in harmonic representations of global heat flow by Pollack et al. (1993) and Chapman and Pollack (1975). The contour values are in units of mW/m^2. Positive values mean that estimates of Pollack et al. (1993) are higher than the estimates by Chapman and Pollack (1975)

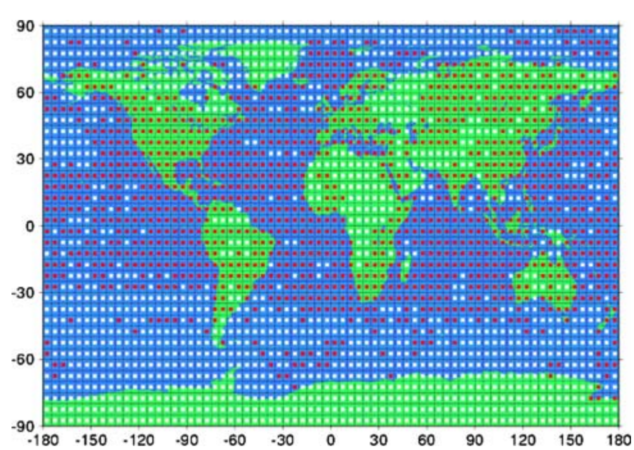

Fig. 3 Grid system used analysis of global heat flow. The *red dots* indicate grid elements for which experimental data are available. The *white dots* indicate grid elements for which estimated values, based on the empirical heat flow–age relation, were used

Subsequent to discretization, fully normalized Legendre coefficients were calculated for 12° spherical harmonic expansion of the homogenized dataset. The basic theory of the method employed in harmonic analysis is well-known (Blakely 1995; Chapman and Bartels 1940). The normalization procedure used in the present work is outlined in Appendix 1. Table 3 lists the new set of coefficients, for harmonic expansion of degree 12. The value of the first coefficient A_{00} and the mean of the individual values of the grid elements are respectively 57.6 and 66.9 mW/m^2. These values indicate that improvements in the database over the last few decades have not lead to significant changes in the mean global conductive heat flow.

The power spectrum of the harmonic coefficients provides further clues as to the nature of large-scale variations in global heat flow. The variation of the root-mean-square (RMS) amplitude, defined as $\left[\sum_m \left(A_{nm}^2 + B_{nm}^2\right)/(2n+1)\right]^{1/2}$, with the degree of harmonic expansion is illustrated in Fig. 4. Note that the amplitudes fall in the rather narrow range of 1–3 mW/m^2, and the decrease of power with harmonic expansion is relatively smooth. Also shown in Fig. 4 are power spectra determined in the earlier works of C&P and PH&J. Note that the harmonic spectrum of the present work is similar to that reported by C&P, but significantly different from that of PH&J.

The revised sets of harmonic coefficients were employed in deriving new global heat flow maps. The public domain computational package, the Generic mapping tool (GMT) (Wessel and Smith 1998), was used. A number of numerical simulations were carried out using the built-in routines available in GMT, the purpose being to assess the influence of gridding and interpolation procedures in map representations. As an example Fig. 5 shows the global heat flow map based on the new set of Legendre coefficients corresponding to harmonic expansion of degree 12. It reveals that the East Pacific and South East Indian Ocean Ridge systems as well as Japan Sea stand out as oceanic regions with heat flux in the range of 100–150 mW/m^2. Ridge systems of the Atlantic, Pacific and Indian Oceans also appear as zones of higher than normal heat flux, but the mean values are in the range of 80–100 mW/m^2. The ocean basins and areas of low angle subduction appear to be characterized by normal heat flux (in the range of 60–80 mW/m^2), whereas the central parts of the continental areas of Africa, Asia, North America, South America, Antarctic and Australia seem to be characterized by relatively low heat flux values (<60 mW/m^2).

The map of Fig. 5 appears, at first sight, to be similar to the one derived in the earlier work by PH&J, but significant differences may easily be noticed on closer examination. For example, the absolute values of conductive heat flow anomalies of the present work are systematically lower

Table 3 Revised set of coefficients (A_{nm} and B_{nm}) for 12° spherical harmonic expansion of conductive heat flow

n	m	A_{nm}	B_{nm}
0	0	61.320	0.000
1	0	–1.207	0.000
1	1	–3.411	–3.295
2	0	–1.740	0.000
2	1	1.073	0.694
2	2	–4.200	1.141
3	0	0.792	0.000
3	1	–0.281	0.029
3	2	1.686	–0.730
3	3	3.140	1.617
4	0	–1.880	0.000
4	1	0.015	–0.091
4	2	1.752	0.566
4	3	–0.250	–0.863
4	4	0.250	–4.441
5	0	1.081	0.000
5	1	–1.116	–0.542
5	2	2.046	0.465
5	3	1.833	–0.643
5	4	–2.900	1.171
5	5	–1.965	–1.708
6	0	–1.447	0.000
6	1	1.034	1.398
6	2	1.558	–1.096
6	3	0.327	–0.354
6	4	–0.793	–0.809
6	5	–0.385	0.437
6	6	0.392	1.904
7	0	0.886	0.000
7	1	0.158	–0.703
7	2	–0.973	0.124
7	3	1.242	–0.409
7	4	0.538	–1.160
7	5	0.112	1.171
7	6	–0.568	0.441
7	7	0.780	–0.551
8	0	1.020	0.000
8	1	–0.094	1.534
8	2	1.434	0.237
8	3	–0.548	–0.270
8	4	–0.158	0.190
8	5	0.838	0.560
8	6	1.255	1.453
8	7	0.555	–0.444
8	8	–0.503	–0.094
9	0	0.261	0.000
9	1	1.183	0.183

Table 3 continued

n	m	A_{nm}	B_{nm}
9	2	0.174	–0.353
9	3	–1.816	–0.991
9	4	0.232	–0.512
9	5	0.168	–0.139
9	6	1.360	0.509
9	7	–0.257	–1.658
9	8	0.707	0.609
9	9	0.252	1.378
10	0	0.402	0.000
10	1	0.980	–0.106
10	2	–0.525	0.321
10	3	0.552	0.008
10	4	–0.888	–0.208
10	5	0.478	0.219
10	6	–0.600	–0.084
10	7	–0.785	0.227
10	8	–0.126	0.143
10	9	0.319	0.512
10	10	1.354	–0.963
11	0	–0.666	0.000
11	1	–0.338	–0.042
11	2	0.320	0.216
11	3	–0.237	–0.050
11	4	0.578	–0.405
11	5	–0.139	1.247
11	6	–0.045	–0.157
11	7	–0.251	–0.045
11	8	0.356	0.187
11	9	0.140	1.321
11	10	0.131	0.050
11	11	–0.129	–0.468
12	0	0.128	0.000
12	1	–0.039	–0.178
12	2	0.033	0.527
12	3	0.808	0.010
12	4	0.091	–0.418
12	5	–0.428	–0.181
12	6	0.749	–0.608
12	7	–0.125	–0.006
12	8	0.122	1.280
12	9	–0.132	0.287
12	10	0.642	–0.899
12	11	0.119	–0.487
12	12	–0.535	0.733

than those of PH&J, in both continental and oceanic regions. Also, major positive anomalies have heat flux values in the range of 100–150 mW/m^2, whereas the ones

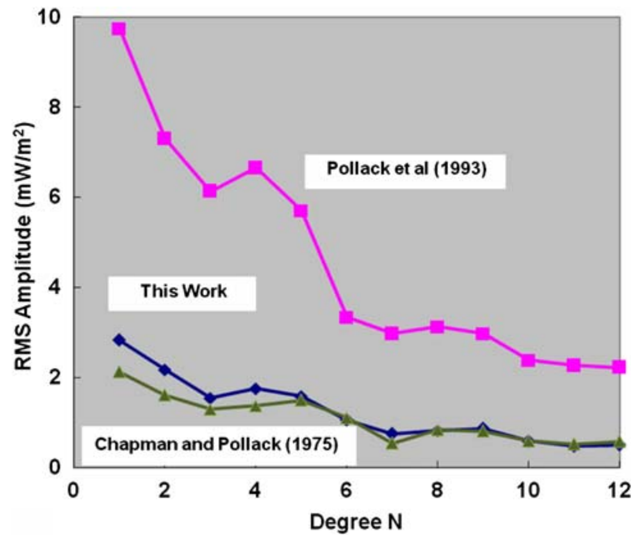

Fig. 4 Comparison of root-mean-square (rms) amplitudes of the harmonic spectra of global heat flow. The *blue curve* refers to the results of the present work. The *green* and *pink curves* refer to spectra obtained by Chapman and Pollack (1975) and Pollack et al. (1993), respectively

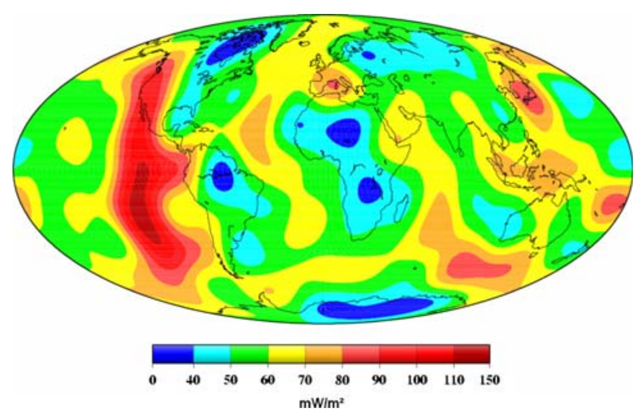

Fig. 5 Global map derived from spherical harmonic expansion to degree 12 of conductive heat flow data. The contour values are in units of mW/m^2

outlined in the earlier work of PH&J have mean heat flux of up to 350 mW/m^2. Figure 6 illustrates the differences between global heat flow representations of the present work and that of PH&J. The regions of major discrepancies are located in the southern hemisphere along the East Pacific Rise, South Mid Atlantic and South East Indian Ocean ridges. Coincidently, these are also the regions for which PH&J made extensive use of theoretical values derived from plate cooling models. The ridge segments in the northern hemisphere also appear as areas with positive differences. In general, the differences seem to be rather systematic, but clearly more pronounced for the oceanic regions. On the other hand, the differences are found to be much less in continental areas, where theoretical values were not employed.

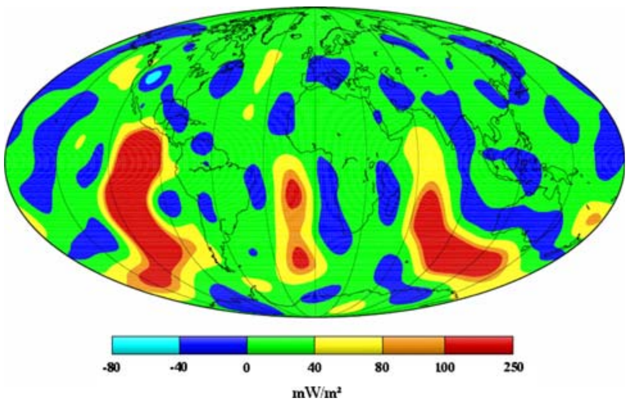

Fig. 6 Map of differences in harmonic representations of global heat flow by Pollack et al. (1993) and that in the present work. The contour values are in units of mW/m^2. Positive values mean that estimates of Pollack et al. (1993) are higher than the estimates of the present work

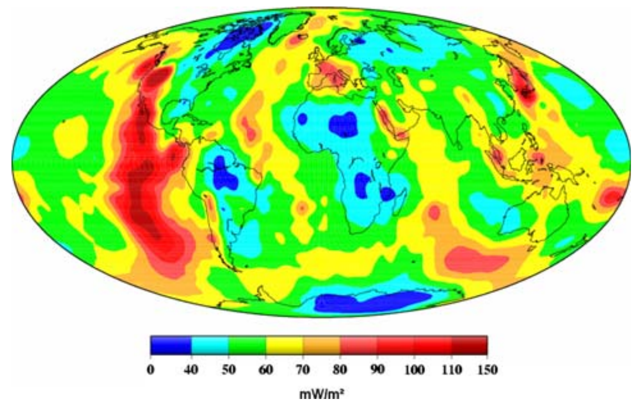

Fig. 7 Global map derived from spherical harmonic expansion to degree 36 of conductive heat flow data. The contour values are in units of mW/m^2

Higher degree harmonic representations

It is a well-known that low degree harmonic representations act as low-pass filters suppressing small-scale variations and enhancing large-scale or regional trends. Obviously, higher degree harmonic expansions are necessary for identifying small-scale variations and also for improving the spatial resolution of large-scale heat flow anomalies. The relation between degree of expansion and spatial resolution may be better understood on the basis of equations used for determination of harmonic coefficients. As demonstrated in Appendix 2 this relation is:

$$m = \frac{\pi}{\Delta\phi} \tag{1}$$

where m is the degree of expansion and $\Delta\phi$ the spatial resolution. According to the above equation the resolution associated with 12° harmonic expansion is 15°, which is equivalent to spatial dimensions of approximately 1,600 km in equatorial regions. It is obvious that 12° representations lack the resolution for identifying heat flow anomalies associated with many of the regional tectonic features whose lateral dimensions are less than 1,600 kilometers.

In the present work, the spherical harmonic expansion has been extended to degree 36 as part of an attempt to improve the spatial resolution of the heat flow anomalies. The spatial resolution in this case reaches up to 5° (equivalent to a few hundred kilometers in equatorial regions), which is comparable to the lateral dimensions of such tectonic features as ocean ridges and cratonic areas. However, the choice of higher degree expansion needs to take into consideration the characteristics of data density and its geographic distribution. For 36° expansion, the number of grid elements for which experimental heat flow data is available is slightly less than 50% of the total. Higher degree expansions would lead to a large number of grid elements with estimated values, making the harmonic representation less reliable. Also, most of the grid elements for which data are available are situated at low latitudes and hence its total surface area is higher than that for grid elements without data. Higher degree expansion would mean a substantial increase in the number grid elements without data at low latitudes. The resulting harmonic representations are likely to be dictated by estimated values rather than by experimental data.

The new set of coefficients, for harmonic expansion of degrees 13–36, is listed in Table 4 of Appendix 3. Note that the harmonic coefficients are independent (orthogonal property of Legendre Polynomials) and hence the set in Table 4 is actually a complement to that provided in Table 3, for harmonic expansions of degrees 1–12.

The set of global heat flow maps derived from coefficients corresponding to harmonic expansions of degrees 1 to 36 reveal that the improvement in spatial resolution of heat flow anomalies is substantial for low harmonics, reaching up to degree 12. In the range corresponding to degrees higher than 12 the improvement is slow but steady. Calculation of RMS amplitudes indicates that the contribution of higher harmonics is approximately 10%. The global heat flow map derived for harmonic expansion of degree 36 is presented in Fig. 7. The outstanding feature of this map is its relatively better resolution, which has allowed significant improvements in outlining the major heat flow anomalies in both continental and oceanic regions. This can easily be seen by comparing the map of Fig. 7 with the map derived from harmonic representation of degree 12 (Fig. 5). Prominent examples are the positive anomalies in East Pacific, South Indian Ocean, and the back-arc regions of the west Pacific. Other examples include the anomalies associated with the ocean ridges in the Atlantic, Pacific, and Indian Oceans where heat flow is higher than normal (generally in the range of 80–100 mW/

m^2). Improvements can also be seen in delimiting low heat flux (<60 mW/m^2) regions in the central parts of the continental areas of Africa, Asia, North America, South America, Antarctic, and Australia.

Discussion

The results obtained in the present work reveal that harmonic representation based on conductive heat flow lead to global heat flow maps that are substantially different from those presented by PH&J. Such differences have potential implications for studies of large-scale variations of heat flow of the earth and also in estimates of the rates of global heat loss. However, lack of direct evidences about the details of hydrothermal processes in the ocean crust makes it difficult to decide which of the representation provides a better approximation of the true heat flow field of the earth. In this context, the harmonic representation of conductive heat flow may be considered as an alternative providing minimum estimates of global heat loss. Nevertheless, the implications of this representation need to be tested against independent lines of evidence concerning the thermal state of the earth's interior. In trying to address this problem we focus the discussion here on the following items that may provide potentially useful information:

1. Comparative analysis of large-scale features discernible in harmonic and numerical representations of regional heat flow; and
2. Independence of the harmonic coefficients and its consequence in low degree representations of heat flow in the oceanic crust.

Comparison between numerical and harmonic representations

Large-scale trends discernible in numerical representations of regional heat flow provide a convenient means of verifying features identified in harmonic representations. Continental areas of Australia and South America were selected for such comparative studies. These are relatively small continents whose regional heat flow fields are relatively well-known (Cull 1982; Hamza and Muñoz 1996; Hamza et al. 2005). In addition, heat flow in upper crustal layers of these continental regions is free of the eventual perturbing effects of hydrothermal circulation of ocean waters. The numerical representation of the regional heat

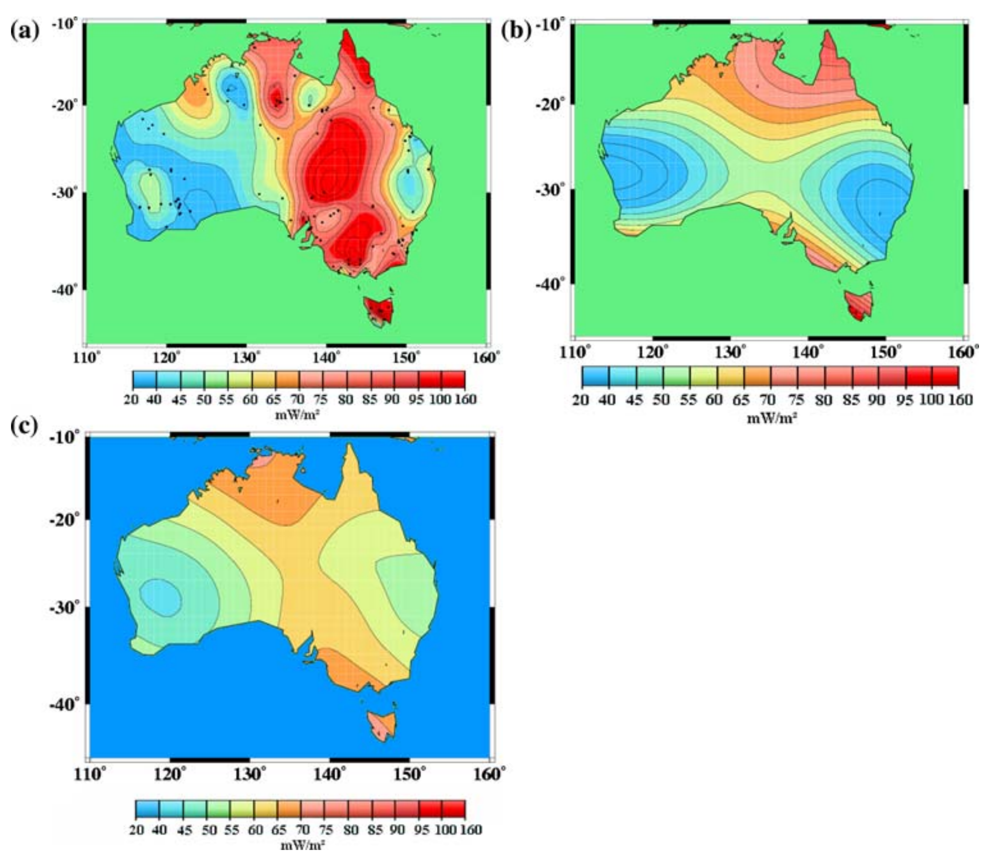

Fig. 8 **a** Numerical representation of regional heat flow in the Australian continental region (Cull 1982; Cardoso and Hamza 2005). **b** Regional heat flow map of the Australian continental region, derived from spherical harmonic expansion to degree 12 of Pollack et al. (1993). **c** Regional heat flow map of the Australian continental region, derived from spherical harmonic expansion to degree 36 of the present work

flow field of Australia, presented in Fig. 8a, indicates a north-south trending belt of high heat flow in its central part and low heat flow areas in the western and eastern parts (Cull and Denham 1979; Cardoso and Hamza 2005). Regional heat flow map based on harmonic representations of PH&J, presented in Fig. 8b, reveal a completely different pattern, pointing to an east–west trending low to normal heat flow. On the other hand, the map derived from harmonic coefficients of the present work (Fig. 8c) is found to be capable of outlining large-scale features similar to the ones encountered in the numerical representation (Fig. 8a).

The numerical representation of the heat flow field of South American continent is illustrated in the map of Fig. 9a. It reveals that heat flow is relatively high in areas along the Andean belt and also in the Patagonian platform. The regional heat flow maps based on harmonic representations of PH&J and of the present work are illustrated in Fig. 9b, c, respectively. Note that the

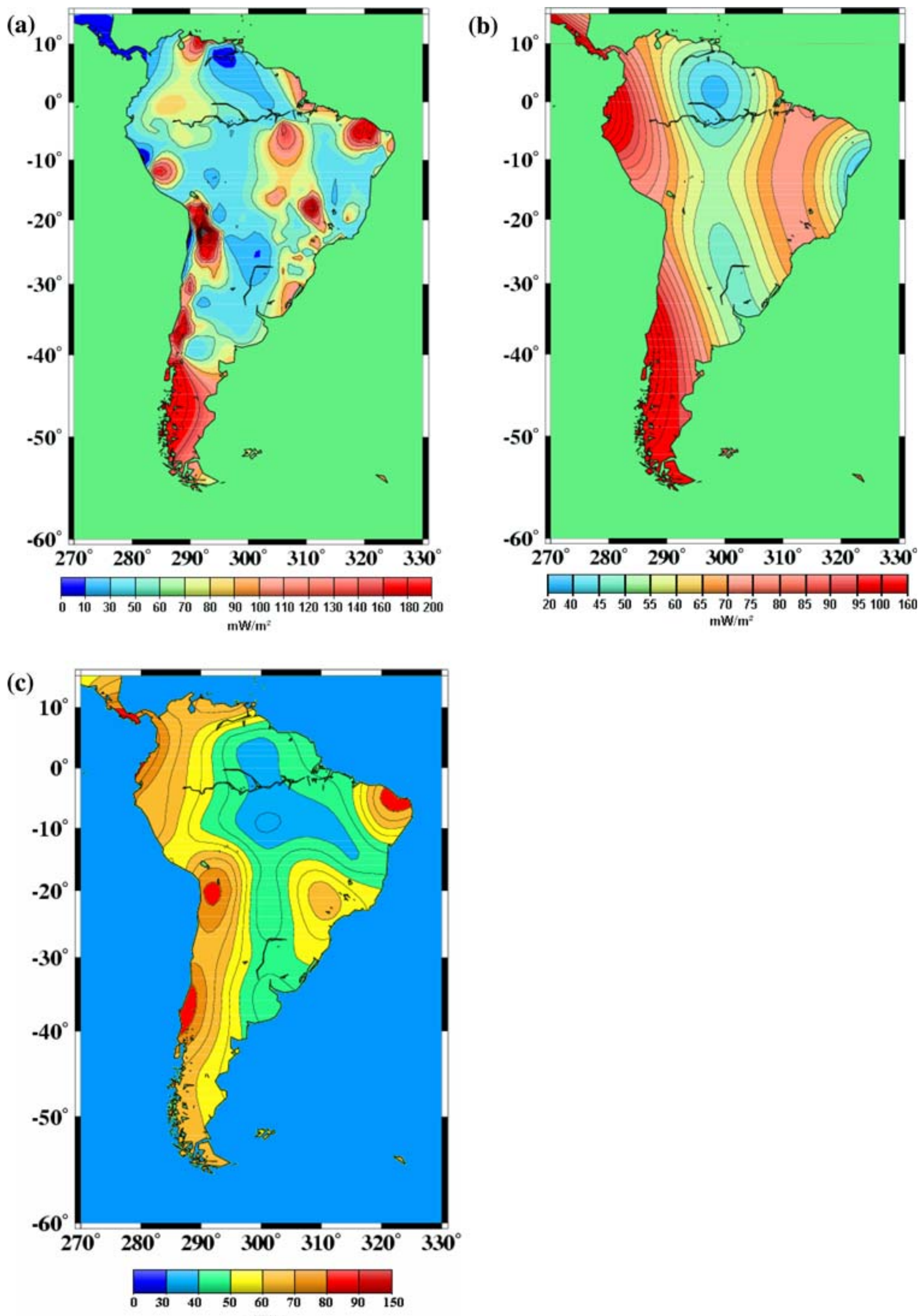

Fig. 9 **a** Numerical representation of regional heat flow in the South American continental region (Hamza et al. 2005; Cardoso and Hamza 2005). **b** Regional heat flow map of the South American continental region, derived from spherical harmonic expansion to degree 12 of Pollack et al. (1993). **c** Regional heat flow map of the South American continental region, derived from spherical harmonic expansion to degree 36 of the present work

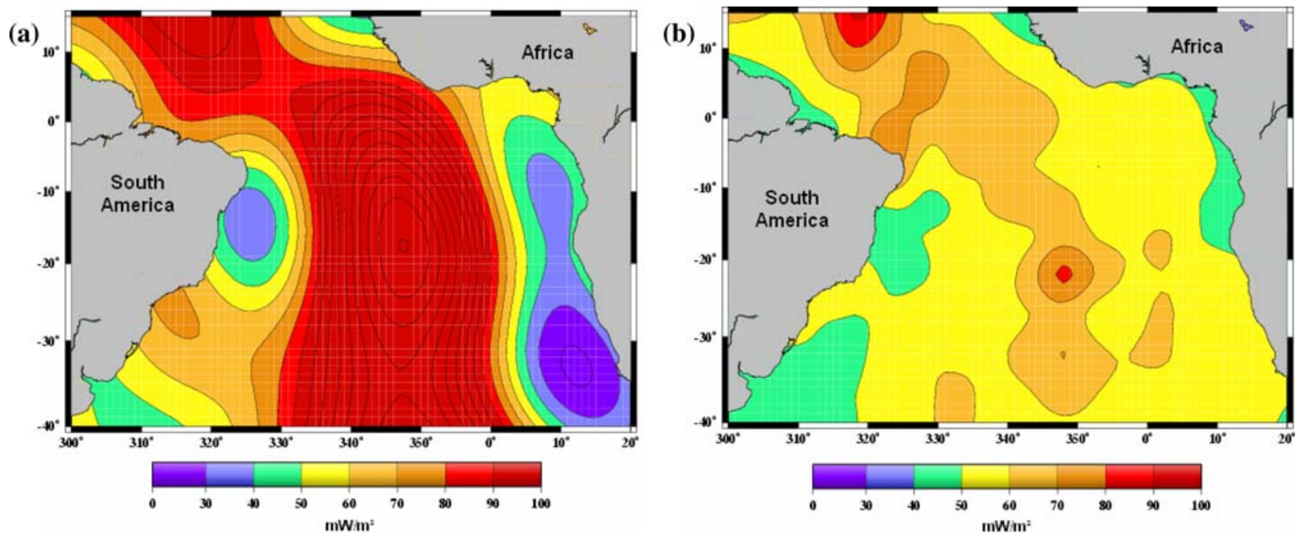

Fig. 10 **a** Regional heat flow map of the Equatorial region of the Atlantic Ocean, derived from the spherical harmonic expansion to degree 12 of Pollack et al. (1993). **c** Regional heat flow map of the Equatorial region of the Atlantic Ocean, derived from the spherical harmonic expansion to degree 36 of the present work

characteristics of regional anomalies of Fig. 9b are considerably different from those present in the map of Fig. 9a. On the other hand the regional features present in harmonic representation of the present work (Fig. 9c) are quite similar to those of the numerical representation (Fig. 9a).

Independence of harmonic coefficients and consequences for low degree representations

The coefficients derived in spherical harmonic analysis are independent (property of orthogonal polynomials) for any particular data set. This is usually considered an important advantage in data analysis (Bevington 1969), but it also has undesirable consequences when modifications are necessary for subsets of data. This can easily be understood by considering the relevant expressions for the harmonic coefficients (see Appendix 1). In the case of discrete data sets the equations for the coefficients are recast as:

$$A_{nm} = \frac{1}{4\pi}\sum_{\phi=0}^{2\pi}\sum_{\theta=0}^{\pi}\overline{q}(\theta,\phi)\cos m\phi\sin\theta \mathrm{P_{nm}}(\cos\theta)\Delta\phi\Delta\theta \tag{2}$$

$$B_{nm} = \frac{1}{4\pi}\sum_{\phi=0}^{2\pi}\sum_{\theta=0}^{\pi}\overline{q}(\theta,\phi)\sin \mathrm{m}\phi\sin\theta \mathrm{P_{nm}}(\cos\theta)\Delta\phi\Delta\theta \tag{3}$$

It is apparent that the values of A_{nm} and B_{nm} depends on the integral over the mean values $q(\theta, \varphi)$ of the grid elements. Consequently, modifications in the dataset for any particular region lead to significant alterations in the entire set of coefficients.

In the work of PH&J, heat flux values for the ridge segments and most of the young ocean crust were upgraded, in an attempt to account for the supposed effect of regional-scale convection heat transfer. However, such upgrading has a direct effect not only on the representation of heat flow in the ocean ridge areas but also that for the remaining regions of the earth, where convective heat transfer is practically insignificant or altogether absent. As an illustrative example consider the heat flow field for the equatorial region of the Atlantic Ocean. The relevant regional heat flow map, derived from the harmonic coefficients of PH&J is presented in Fig. 10a. Note the presence of a rather very broad heat flow anomaly (with values in excess of 80 mW/m^2) over much of the oceanic crust in the central Atlantic region. Such high high heat flow anomalies are incompatible with the experimental heat flow data for this region (Sclater et al. 1980; Cardoso and Hamza 2006). The unavoidable conclusion is that upgrading heat flow in ridge areas has lead to overestimates of heat flow in older segments of the ocean crust where perturbing effects of hydrothermal circulation is negligible or altogether absent.

For comparison purposes we present in Fig. 10b the regional heat flow map of the same region derived from the new set of coefficients for the 36° harmonic expansion of the present work. Note that heat flux in excess of 80 mW/m^2 is encountered only along a narrow belt that encompasses the axial region of the mid Atlantic ridge. The off-ridge parts of the oceanic regions and continental margins have heat flux values of less than 60 mW/m^2. Thus the overall picture is in much better agreement with the experimental data set and the mean values calculated by Sclater et al. (1980) and Cardoso and Hamza (2006).

Conclusions

Harmonic analysis, with due emphasis on experimental heat flow values, has lead to results that are significantly different from that presented in the earlier work of PH&J. Our results are compatible with the characteristics of crustal thermal fields outlined in regional studies. The mean global heat flow is found to fall in the range of 56–67 mW/m^2. These estimates are markedly lower than the global mean of 87 mW/m^2 calculated by PH&J. On the other hand, the range is in reasonable agreement with the mean value of 63 mW/m^2, determined recently by Hofmeister and Criss (2005) on the basis of geochemical arguments.

The results obtained also allow new estimates of global heat loss. The values of global heat loss based on the first coefficient (A_{00}) and integration of binned data are respectively 28.6 and 34.1 TW. These estimates are found to bracket the value proposed by Hofmeister and Criss (2005). Again, our estimates are found to be significantly lower than the value of 44.2 TW obtained by PH&J.

Acknowledgments The second author of this paper has been recipient of a Masters Degree scholarship granted by Coordenadoria de Aperfeiçoamento de Pesquisa e Ensino Superior (CAPES), during the period of 2004–2006. The authors thank Anne Hofmeister (Washington University) for fruitful exchange of information on assessment of global heat flow. Paul Shen (University of Western Ontario) and Vladimir Shukovski (University of São Paulo) provided helpful comments on the subject matter of spherical harmonic representation. Thanks are also due to Iris Escobar (Observatório Nacional) for institutional support.

Appendix 1

Harmonic coefficients and the normalization procedure

The harmonic representation of heat flow (q) in near surface layers is usually expressed as:

$$q(\theta,\phi) = \sum_{n=0}^{N}\sum_{m=0}^{n}[A_{nm}\cos(m\phi) + B_{nm}\sin(m\phi)]P'_{nm}(\cos\theta) \tag{4}$$

where ϕ is the longitude θ = 90 – ψ, is the colatitude, P'_{nm} (cos θ) is the associated Legendre function that is fully normalized and A_{nm} and B_{nm} the coefficients of the harmonic expansion. The expression for evaluation of P'_{nm} is:

$$P_{nm} = \frac{P_{nm}}{\sqrt{K_n^m}} \tag{5}$$

where P_{nm} is the associated Legendre function given by:

$$P_{nm}(\cos\theta) = \frac{\sin^m\theta}{2^n}\sum_{t=0}^{Int\left(\frac{n-m}{2}\right)}\frac{(-1)^t(2n-2t)!}{t!(n-t)!(n-m-2t)!}\cos^{(n-m-2t)}\theta \tag{6}$$

and

$$K_n^m = \frac{1}{H(2n+1)}\frac{(n+m)!}{(n-m)!},\ \begin{cases}\text{if m} = 0 \Rightarrow \text{H} = 0\\ \text{if m} \neq 0 \Rightarrow \text{H} = 2\end{cases} \tag{7}$$

In Eq. (6) *Int[(n–m)/2]* refers to the largest integer that is lower than *(n–m)/2*.

Full normalization of associated Legendre functions (P_{nm}) requires that the following equations be satisfied:

$$\int_0^{2\pi}\int_0^{\pi}\left[P'_{nm}(\cos\theta)\sin(m\phi)\right]^2\sin\theta\,\mathrm{d}\theta\,\mathrm{d}\phi = 4\pi \tag{8a}$$

$$\int_0^{2\pi}\int_0^{\pi}\left[P'_{nm}(\cos\theta)\cos(m\phi)\right]^2\sin\theta\,\mathrm{d}\theta\,\mathrm{d}\phi = 4\pi \tag{8b}$$

The coefficients A_{nm} and B_{nm} are evaluated by fitting the harmonic expansion to the set of experimental data, which are the heat flow values (q) and their respective geographic coordinates (ϕ and θ).

Appendix 2

Relation between degree of harmonic expansion and spatial resolution

A discrete distribution of N data points over the surface of the earth at a specific latitude (θ_0) and spaced at an angular distance of $\Delta\Phi$ follow the relation:

$$N = \frac{2\pi}{\Delta\phi} \tag{9}$$

A function $\overline{q}(\theta_0,\phi)$ which represents heat flow at a specific latitude θ_0, but continuous in ϕ between 0 and 2π may be represented as Fourier sine series:

$$\overline{q}(\theta_o,\phi) = \sum_{m=0}^{\infty}(a_m(\theta_o)\cos m\phi + b_m(\theta_o)\sin m\phi) \tag{10}$$

The coefficients a_m (θ_0) and b_m (θ_0) are calculated using discretized values experimental heat flow ($q(\phi)$) uniformly distributed over the surface of the earth with angular spacing of $\Delta\varphi$. The expressions for the calculation of the coefficients are:

$$a_m(\theta_0) = \frac{2}{N}\sum_{t=1}^{N} q_t(\phi)\cos\left(\frac{2\pi mt}{N}\right) \tag{11}$$

$$b_m(\theta_0) = \frac{2}{N}\sum_{t=1}^{N} q_t(\phi)\sin\left(\frac{2\pi mt}{N}\right) \tag{12}$$

Obviously when $\overline{q}(\phi) = q(\phi)$ Eq. (10) will represent the exact value of the discretized heat flux. This condition allows determination of the "m" to be used in the expansion. The result may be obtained as follows:

1. Substitute Eqs. (11) and (12) in Eq. (10):

$$\begin{aligned}\overline{q}(\theta_0,\phi) = \sum_{m=0}^{\infty}\Bigg(&\frac{2}{N}\sum_{t=1}^{N} q_t(\phi)\cos\left(\frac{2\pi mt}{N}\right)\cos(m\phi)\\ &+\frac{2}{N}\sum_{t=1}^{N} q_t(\phi)\sin\left(\frac{2\pi mt}{N}\right)\sin(m\phi)\Bigg)\end{aligned} \tag{13}$$

2. Substitute Eq. (9) in Eq. (13):

$$\begin{aligned}\overline{q}(\theta_0,\phi) = \frac{2}{N}\sum_{m=0}^{\infty}\Bigg(&\sum_{t=1}^{N} q_t(\phi)\cos(mt\Delta\phi)\cos(m\phi)\\ &+\sum_{t=1}^{N} q_t(\phi)\sin(mt\Delta\phi)\sin(m\phi)\Bigg)\end{aligned} \tag{14}$$

3. The longitude "ϕ_k" may be represented as $\phi_i = k\Delta\phi$, where k is a natural number, so after substitution we have:

$$\begin{aligned}\overline{q}_k(\theta_0,k\Delta\phi) = \frac{2}{N}\sum_{m=0}^{\infty}\Bigg(&\sum_{t=1}^{N} q_t(k\Delta\phi)\cos(mt\Delta\phi)\cos(mk\Delta\phi)\\ &+\sum_{t=1}^{N} q_t(k\Delta\phi)\sin(mt\Delta\phi)\sin(mk\Delta\phi)\Bigg)\end{aligned}$$

4. By the principle of orthogonality, the product cos $(mt\Delta\phi)$ cos $(mk\Delta\phi)$ is non-zero only for $t = k$. Thus all the summation terms become zero except for the term "k", and so we have:

$$\begin{aligned}\overline{q}_k(\theta_0,k\Delta\phi) = \frac{2}{N}\sum_{m=0}^{\infty}(&q_k(k\Delta\phi)\cos(mk\Delta\phi)\cos(mk\Delta\phi)\\ &+q_k(k\Delta\phi)\sin(mt\Delta\phi)\sin(mk\Delta\phi))\end{aligned}$$

$$\begin{aligned}\overline{q}_k(\theta_0,k\Delta\phi) = \frac{2}{N}\sum_{m=0}^{\infty}(&q_k(k\Delta\phi)\cos^2(mk\Delta\phi)\\ &+q_k(k\Delta\phi)\mathrm{sen}^2(\mathrm{mt}\Delta\phi))\end{aligned}$$

which, upon simplification leads to:

$$\overline{q}_k(\theta_0,k\Delta\phi) = \frac{2}{N}\sum_{m=0}^{\infty} q_k(k\Delta\phi)$$

5. Applying the property of summation:

$$\overline{q}_k(\theta_0,k\Delta\phi) = \frac{2}{N} m q_k(k\Delta\phi)$$

6. As $\overline{q}_k(\theta_0,k\Delta\phi)$ must be equal to $q_k\ (k\Delta\phi)$ we have: $1 = \frac{2}{N}m$ which, after substitution of Eq. (9), leads to:

$$m = \frac{\pi}{\Delta\phi}$$

Appendix 3

Table 4.

Table 4 Coefficients for harmonic expansion of degree 36

n	*m*	Anm	Bnm
13	0	–0.113	0.000
13	1	0.079	0.271
13	2	0.043	0.360
13	3	0.022	0.230
13	4	0.068	0.004
13	5	0.062	–0.263
13	6	–0.414	–0.207
13	7	0.123	–0.122
13	8	–0.054	0.481
13	9	0.110	0.344
13	10	0.086	–0.096
13	11	–0.223	–0.185
13	12	–0.119	0.578
13	13	0.011	–0.024
14	0	0.038	0.000
14	1	–0.088	0.264
14	2	–0.007	0.044
14	3	0.300	0.146
14	4	0.051	–0.341
14	5	0.185	–0.272
14	6	–0.284	–0.181
14	7	0.051	0.062
14	8	–0.041	0.159
14	9	–0.027	0.135
14	10	0.118	–0.314
14	11	0.053	–0.074
14	12	–0.306	0.159
14	13	0.107	0.070
14	14	0.026	–0.130
15	0	0.200	0.000
15	1	–0.057	0.097
15	2	0.223	–0.391
15	3	0.156	0.069

Table 4 continued

n	*m*	Anm	Bnm
15	4	–0.092	–0.404
15	5	0.046	–0.120
15	6	–0.131	–0.245
15	7	–0.067	0.255
15	8	–0.028	0.087
15	9	–0.074	0.199
15	10	–0.103	–0.135
15	11	–0.093	0.162
15	12	–0.012	0.296
15	13	–0.062	0.260
15	14	–0.010	–0.291
15	15	–0.390	0.226
16	0	0.322	0.000
16	1	0.081	–0.114
16	2	0.172	–0.200
16	3	–0.109	0.065
16	4	0.001	–0.099
16	5	–0.127	–0.001
16	6	0.009	0.039
16	7	–0.300	0.196
16	8	0.157	–0.051
16	9	0.118	–0.135
16	10	0.227	0.098
16	11	–0.189	0.283
16	12	–0.006	0.170
16	13	0.129	–0.020
16	14	–0.173	–0.082
16	15	–0.227	–0.275
16	16	–0.062	0.185
17	0	–0.030	0.000
17	1	–0.011	–0.286
17	2	–0.135	0.118
17	3	–0.117	–0.121
17	4	0.154	0.262
17	5	–0.139	0.066
17	6	0.138	0.354
17	7	–0.215	0.009
17	8	0.161	–0.167
17	9	0.078	–0.443
17	10	0.246	0.317
17	11	–0.171	0.119
17	12	–0.015	0.119
17	13	0.197	–0.363
17	14	–0.065	–0.013
17	15	–0.053	0.088
17	16	0.048	0.212
17	17	0.462	0.013
18	0	–0.093	0.000

Table 4 continued

n	*m*	Anm	Bnm
18	1	–0.121	–0.148
18	2	–0.105	0.035
18	3	–0.064	–0.114
18	4	–0.101	0.225
18	5	0.029	0.023
18	6	0.080	0.173
18	7	0.035	–0.097
18	8	–0.030	–0.089
18	9	–0.166	–0.175
18	10	–0.074	0.153
18	11	–0.218	0.134
18	12	–0.008	–0.162
18	13	0.154	–0.374
18	14	–0.101	0.109
18	15	–0.314	0.116
18	16	0.365	–0.012
18	17	0.316	–0.031
18	18	0.063	–0.142
19	0	0.007	0.000
19	1	–0.002	0.016
19	2	–0.103	0.087
19	3	–0.034	0.207
19	4	–0.177	0.140
19	5	0.093	0.032
19	6	0.023	–0.087
19	7	–0.058	–0.208
19	8	–0.132	–0.125
19	9	–0.066	0.045
19	10	–0.156	0.126
19	11	–0.069	0.197
19	12	0.006	–0.015
19	13	0.264	–0.035
19	14	–0.084	–0.043
19	15	–0.034	0.097
19	16	0.084	–0.123
19	17	0.032	–0.203
19	18	0.191	–0.301
19	19	–0.278	0.013
20	0	0.116	0.000
20	1	0.062	0.008
20	2	–0.075	0.218
20	3	0.124	0.232
20	4	0.180	0.227
20	5	0.111	–0.004
20	6	0.025	–0.052
20	7	–0.072	–0.176
20	8	–0.131	–0.162
20	9	0.029	0.053

Table 4 continued

n	*m*	Anm	Bnm
20	10	–0.149	0.262
20	11	0.057	0.008
20	12	0.125	0.092
20	13	0.216	–0.135
20	14	–0.054	–0.099
20	15	0.018	0.103
20	16	0.177	–0.243
20	17	0.085	–0.139
20	18	–0.382	–0.411
20	19	–0.122	–0.158
20	20	0.122	0.183
21	0	–0.111	0.000
21	1	–0.084	0.159
21	2	0.033	0.006
21	3	0.139	–0.035
21	4	0.229	0.099
21	5	0.127	–0.150
21	6	0.075	–0.061
21	7	0.028	–0.037
21	8	–0.308	0.038
21	9	–0.044	0.080
21	10	–0.104	0.157
21	11	0.183	–0.208
21	12	0.098	–0.022
21	13	0.082	0.206
21	14	–0.272	–0.024
21	15	0.004	0.009
21	16	0.322	0.016
21	17	–0.211	–0.069
21	18	0.041	0.029
21	19	0.002	0.121
21	20	–0.036	0.095
21	21	0.226	0.012
22	0	0.183	0.000
22	1	–0.091	0.220
22	2	0.125	–0.286
22	3	0.016	–0.122
22	4	0.011	–0.203
22	5	0.010	–0.122
22	6	–0.107	–0.230
22	7	–0.022	–0.005
22	8	–0.317	0.136
22	9	–0.006	0.129
22	10	0.048	–0.076
22	11	0.223	–0.068
22	12	–0.048	–0.081
22	13	0.037	0.344
22	14	–0.129	–0.187

Table 4 continued

n	*m*	Anm	Bnm
22	15	0.017	–0.064
22	16	0.382	–0.020
22	17	–0.103	0.048
22	18	–0.182	0.143
22	19	0.544	–0.042
22	20	0.085	0.314
22	21	–0.064	0.029
22	22	–0.031	–0.093
23	0	0.203	0.000
23	1	0.025	–0.085
23	2	0.107	–0.227
23	3	–0.035	–0.053
23	4	–0.051	–0.236
23	5	–0.115	0.106
23	6	–0.239	–0.166
23	7	–0.049	0.067
23	8	–0.033	0.018
23	9	0.097	0.130
23	10	0.048	–0.168
23	11	0.125	0.175
23	12	–0.147	–0.242
23	13	–0.086	0.098
23	14	0.196	–0.249
23	15	0.093	0.099
23	16	0.427	0.108
23	17	–0.186	0.191
23	18	–0.144	–0.108
23	19	0.170	0.067
23	20	0.269	–0.196
23	21	–0.086	0.142
23	22	–0.073	0.125
23	23	–0.181	–0.105
24	0	0.175	0.000
24	1	–0.037	–0.229
24	2	0.011	–0.073
24	3	–0.003	–0.077
24	4	0.020	–0.033
24	5	–0.171	0.258
24	6	0.037	–0.011
24	7	–0.037	0.102
24	8	0.254	–0.002
24	9	–0.063	0.144
24	10	0.207	–0.116
24	11	–0.147	0.186
24	12	–0.062	–0.093
24	13	–0.417	–0.014
24	14	0.151	–0.073
24	15	–0.027	0.108

Table 4 continued

n	*m*	Anm	Bnm
24	16	0.040	–0.061
24	17	–0.143	0.014
24	18	–0.136	0.058
24	19	0.102	0.002
24	20	0.105	0.104
24	21	–0.461	–0.186
24	22	0.127	0.224
24	23	–0.037	0.184
24	24	–0.209	0.015
25	0	–0.019	0.000
25	1	–0.038	–0.014
25	2	–0.054	0.058
25	3	–0.035	–0.082
25	4	–0.068	0.082
25	5	–0.101	0.084
25	6	0.226	0.055
25	7	0.047	0.023
25	8	0.278	0.073
25	9	–0.149	0.125
25	10	–0.044	0.037
25	11	–0.147	–0.034
25	12	–0.144	0.334
25	13	–0.050	–0.064
25	14	0.142	0.101
25	15	0.025	0.025
25	16	–0.073	0.149
25	17	–0.017	–0.373
25	18	–0.039	0.144
25	19	0.399	–0.038
25	20	–0.257	0.021
25	21	0.088	0.031
25	22	–0.189	0.216
25	23	0.212	0.138
25	24	0.091	–0.065
25	25	0.076	0.117
26	0	0.200	0.000
26	1	–0.039	0.056
26	2	–0.193	0.158
26	3	–0.076	–0.045
26	4	–0.049	0.032
26	5	0.105	–0.119
26	6	0.140	0.052
26	7	0.193	–0.148
26	8	0.103	–0.056
26	9	–0.080	–0.126
26	10	–0.257	0.032
26	11	–0.163	0.008
26	12	–0.028	0.156

Table 4 continued

n	*m*	Anm	Bnm
26	13	0.190	0.012
26	14	0.269	0.057
26	15	0.123	–0.028
26	16	–0.002	0.209
26	17	0.027	–0.471
26	18	–0.061	0.169
26	19	0.171	–0.123
26	20	–0.250	–0.213
26	21	–0.066	0.021
26	22	0.097	0.133
26	23	0.148	0.117
26	24	–0.118	–0.171
26	25	0.132	–0.225
26	26	0.161	0.063
27	0	–0.002	0.000
27	1	–0.007	–0.020
27	2	–0.102	0.036
27	3	–0.115	–0.028
27	4	0.014	0.073
27	5	0.132	0.016
27	6	0.029	0.036
27	7	0.130	–0.220
27	8	–0.009	–0.212
27	9	–0.048	–0.227
27	10	–0.154	–0.077
27	11	–0.103	0.184
27	12	0.055	–0.075
27	13	0.043	0.055
27	14	0.102	–0.027
27	15	–0.018	–0.080
27	16	0.046	–0.030
27	17	0.217	–0.231
27	18	–0.020	0.108
27	19	0.084	0.263
27	20	–0.331	–0.088
27	21	–0.294	–0.137
27	22	0.169	0.173
27	23	–0.171	0.165
27	24	–0.050	–0.334
27	25	–0.199	0.083
27	26	–0.082	–0.139
27	27	–0.165	–0.009
28	0	0.142	0.000
28	1	0.060	0.059
28	2	0.014	0.006
28	3	0.150	–0.034
28	4	0.089	0.037
28	5	0.070	0.008

Table 4 continued

n	*m*	Anm	Bnm
28	6	0.021	0.068
28	7	0.032	–0.077
28	8	–0.126	–0.100
28	9	–0.091	–0.106
28	10	–0.001	0.099
28	11	0.032	0.038
28	12	0.166	0.156
28	13	0.069	–0.141
28	14	–0.013	0.104
28	15	–0.155	–0.136
28	16	0.007	–0.025
28	17	0.201	0.030
28	18	–0.058	0.143
28	19	0.116	0.281
28	20	–0.119	–0.152
28	21	–0.234	0.010
28	22	0.059	0.047
28	23	–0.052	–0.121
28	24	–0.126	–0.148
28	25	–0.220	–0.238
28	26	0.088	0.155
28	27	–0.114	–0.039
28	28	0.144	0.047
29	0	0.059	0.000
29	1	0.233	0.192
29	2	–0.013	0.034
29	3	0.199	0.020
29	4	0.094	–0.085
29	5	0.054	–0.149
29	6	–0.070	0.025
29	7	0.023	–0.090
29	8	–0.093	0.053
29	9	–0.010	–0.037
29	10	0.149	0.288
29	11	0.161	0.053
29	12	0.014	0.143
29	13	0.048	–0.201
29	14	–0.097	0.008
29	15	–0.151	–0.241
29	16	0.050	–0.078
29	17	0.227	0.071
29	18	–0.077	0.162
29	19	0.032	0.025
29	20	0.145	–0.206
29	21	–0.085	0.096
29	22	0.181	–0.030
29	23	–0.030	–0.133
29	24	0.059	–0.136

Table 4 continued

n	*m*	Anm	Bnm
29	25	–0.022	–0.079
29	26	–0.228	0.039
29	27	0.365	–0.194
29	28	–0.051	–0.051
29	29	0.158	0.039
30	0	0.196	0.000
30	1	0.148	0.094
30	2	0.114	–0.015
30	3	–0.075	0.094
30	4	0.003	–0.175
30	5	–0.021	–0.108
30	6	–0.181	–0.140
30	7	–0.093	–0.077
30	8	0.025	0.049
30	9	0.218	–0.080
30	10	0.083	0.062
30	11	0.224	0.095
30	12	–0.061	–0.081
30	13	–0.057	–0.090
30	14	–0.171	–0.113
30	15	0.016	–0.026
30	16	–0.040	–0.140
30	17	0.215	0.060
30	18	–0.081	0.156
30	19	–0.013	0.043
30	20	0.087	–0.234
30	21	–0.019	0.238
30	22	0.069	–0.022
30	23	–0.171	–0.268
30	24	0.173	–0.057
30	25	0.079	0.104
30	26	0.001	0.045
30	27	–0.038	–0.197
30	28	0.036	–0.136
30	29	0.023	0.008
30	30	–0.128	–0.057
31	0	0.009	0.000
31	1	–0.109	–0.184
31	2	0.129	–0.010
31	3	–0.004	0.082
31	4	0.046	–0.150
31	5	–0.136	0.096
31	6	–0.075	–0.173
31	7	–0.035	0.062
31	8	0.100	–0.096
31	9	0.165	0.055
31	10	–0.031	–0.085
31	11	0.105	–0.004

Table 4 continued

n	*m*	Anm	Bnm
31	12	–0.010	–0.048
31	13	0.130	0.034
31	14	–0.193	–0.034
31	15	0.201	0.262
31	16	–0.136	–0.011
31	17	0.030	0.010
31	18	–0.186	0.060
31	19	0.176	–0.065
31	20	0.058	–0.152
31	21	–0.122	0.204
31	22	0.074	0.166
31	23	–0.157	–0.170
31	24	0.027	–0.074
31	25	0.112	0.217
31	26	–0.073	–0.264
31	27	0.123	–0.130
31	28	0.120	0.074
31	29	–0.205	–0.070
31	30	0.081	–0.097
31	31	–0.012	0.026
32	0	0.228	0.000
32	1	–0.018	–0.175
32	2	0.005	0.054
32	3	–0.004	0.055
32	4	–0.022	–0.042
32	5	–0.003	0.006
32	6	0.088	–0.116
32	7	0.077	0.136
32	8	0.194	–0.203
32	9	–0.003	0.185
32	10	–0.013	–0.101
32	11	–0.064	–0.010
32	12	–0.181	0.006
32	13	0.137	0.190
32	14	0.033	0.025
32	15	0.173	0.163
32	16	0.027	–0.010
32	17	–0.044	0.094
32	18	–0.112	–0.262
32	19	0.038	0.096
32	20	0.036	–0.103
32	21	–0.165	0.177
32	22	0.005	0.152
32	23	0.024	–0.354
32	24	–0.037	–0.014
32	25	0.077	0.218
32	26	–0.076	–0.078
32	27	–0.024	–0.263

Table 4 continued

n	*m*	Anm	Bnm
32	28	0.230	–0.134
32	29	0.109	0.132
32	30	0.131	0.142
32	31	–0.024	0.041
32	32	0.073	0.128
33	0	0.064	0.000
33	1	–0.026	0.042
33	2	0.031	0.043
33	3	–0.135	–0.005
33	4	–0.103	0.177
33	5	0.073	–0.104
33	6	–0.026	0.069
33	7	–0.100	0.159
33	8	0.157	–0.063
33	9	–0.016	0.015
33	10	0.057	–0.231
33	11	–0.214	0.034
33	12	0.052	0.019
33	13	–0.101	0.189
33	14	0.175	0.036
33	15	0.080	–0.004
33	16	0.002	–0.015
33	17	–0.060	–0.027
33	18	–0.023	–0.177
33	19	0.066	0.054
33	20	0.053	–0.004
33	21	–0.219	0.125
33	22	0.124	0.008
33	23	0.036	–0.173
33	24	–0.048	–0.084
33	25	0.332	0.004
33	26	–0.103	0.028
33	27	0.154	–0.103
33	28	–0.026	0.172
33	29	0.023	0.057
33	30	0.270	–0.270
33	31	0.136	0.189
33	32	–0.171	0.226
33	33	–0.110	–0.012
34	0	0.118	0.000
34	1	–0.216	–0.006
34	2	–0.077	–0.046
34	3	–0.042	–0.094
34	4	0.108	0.266
34	5	–0.005	0.062
34	6	0.041	0.173
34	7	–0.033	–0.022
34	8	0.039	0.005

Table 4 continued

n	*m*	Anm	Bnm
34	9	0.046	–0.034
34	10	0.020	–0.126
34	11	–0.212	–0.006
34	12	0.233	0.047
34	13	–0.124	0.079
34	14	0.106	0.008
34	15	0.003	–0.084
34	16	0.057	–0.109
34	17	–0.108	–0.094
34	18	0.030	0.101
34	19	0.032	–0.072
34	20	0.020	0.277
34	21	–0.240	0.077
34	22	0.274	0.065
34	23	0.099	–0.233
34	24	–0.207	0.075
34	25	0.112	–0.104
34	26	–0.075	–0.321
34	27	0.350	0.058
34	28	0.019	–0.024
34	29	0.013	0.089
34	30	0.018	0.015
34	31	–0.038	0.060
34	32	0.071	–0.025
34	33	0.103	0.118
34	34	–0.088	–0.089
35	0	–0.248	0.000
35	1	–0.006	0.006
35	2	–0.146	–0.080
35	3	0.051	–0.024
35	4	0.160	0.085
35	5	0.074	0.119
35	6	0.265	0.076
35	7	0.098	–0.165
35	8	–0.055	–0.030
35	9	0.129	–0.209
35	10	0.070	0.068
35	11	–0.038	–0.061
35	12	–0.015	0.187
35	13	–0.021	0.121
35	14	0.173	0.007
35	15	–0.029	–0.172
35	16	0.143	–0.091
35	17	–0.102	–0.168
35	18	0.019	0.101
35	19	–0.134	–0.079
35	20	–0.043	0.204
35	21	0.055	–0.018

Table 4 continued

n	*m*	Anm	Bnm
35	22	0.109	0.109
35	23	0.253	–0.283
35	24	–0.272	0.188
35	25	0.056	–0.065
35	26	0.021	–0.136
35	27	0.026	0.041
35	28	0.087	–0.033
35	29	–0.055	–0.138
35	30	0.028	–0.017
35	31	0.175	0.087
35	32	–0.448	0.036
35	33	0.019	–0.138
35	34	0.195	–0.077
35	35	–0.043	0.071
36	0	0.188	0.000
36	1	0.231	0.062
36	2	–0.028	–0.014
36	3	0.053	0.084
36	4	0.013	0.048
36	5	0.192	0.044
36	6	0.041	0.017
36	7	0.022	–0.212
36	8	–0.068	0.011
36	9	0.069	–0.420
36	10	0.043	0.059
36	11	0.134	–0.020
36	12	–0.164	0.099
36	13	0.040	0.019
36	14	0.153	–0.017
36	15	0.072	–0.106
36	16	0.107	0.128
36	17	–0.091	–0.125
36	18	0.103	0.015
36	19	–0.161	–0.214
36	20	–0.009	–0.016
36	21	0.129	–0.159
36	22	0.063	0.145
36	23	0.047	0.007
36	24	–0.198	0.180
36	25	0.128	0.029
36	26	0.090	–0.232
36	27	–0.149	0.074
36	28	0.047	0.207
36	29	–0.360	–0.341
36	30	0.064	0.014
36	31	–0.034	0.053
36	32	0.003	0.139
36	33	–0.245	0.132

Table 4 continued

n	*m*	Anm	Bnm
36	34	–0.178	0.053
36	35	0.082	–0.189
36	36	0.000	0.039

References

Akaku K (1988) Geochemistry of mineral deposition from geothermal waters: deposition processes of common minerals found in various geothermal fields and case study in the Fushime geothermal field. J Jpn Geothermal Energy Assoc 25:154–171

Alexandrino CH, Hamza VM (2005) A simple semi-analytical model for estimating heat flow variations in hydrothermal areas. IASPEI Regional Assembly, Santiagom

Baker ET, Chen YJ, Morgan JP (1996) The relationship between near-axis hydrothermal cooling and the spreading rate of mid-ocean ridges. Earth Planet Sci Lett 142:137–145

Balling N, Haenel R, Ungemach P, Vasseur G, Whieldon J (1981) Preliminary guidelines for heat flow density determination. Energy Commission of the European Communities, Luxemburg, Catalogue No. CD-ND-81-068-EN-C, pp 32

Becker K, Davis E (2003) New evidence for age variation and scale effects of permeabilities of young oceanic crust from borehole thermal and pressure measurements. Earth Planet Sci Lett 201:499–508

Becker K, Fisher A (2000) Permeability of upper oceanic basement on the eastern flank of the Endeavor Ridge determined with drill-string packer experiments. J Geophys Res 105(B1):897–912

Bevington PR (1969) Data reduction and error analysis for the physical sciences. McGraw-Hill, New York, pp 1–336

Birch F (1954) The present state of geothermal investigations. Geophysics 19:645–659

Blakely RJ (1995) Potential theory in gravity and magnetic applications. Cambridge University Press, Cambridge

Bryant WR, Bennett RH, Katherman CE (1981) Shear strength, consolidation, porosity and permeability of oceanic sediments. In: Emiliani C (eds) The oceanic lithosphere. Wiley, New York, pp 1555–1616

Cardoso RR (2006) Analytic representation of the global thermal field by the method of spherical harmonics (in Portuguese), Unpublished M.Sc. Thesis, Observatório Nacional–MCT, Rio de Janeiro, Brazil

Cardoso RR, Hamza VM (2006) Crustal heat flow variations of in the Equatorial Atlantic: implications for geothermal structure of NE Brazil. In: Proceedings of the 2nd symposium of the Brazilian Geophysical Society, Natal, p 6

Cardoso RR, Hamza VM (2005) A comparative analysis of numerical and harmonic representations of conductive heat flow in the South American and Australian continents (Abstract). IASPEI Regional Assembly, Santiago

Cardoso RR, Ponte Neto CF, Hamza VM (2005) A reappraisal of global heat flow data. In: Proceedings of the 9th international congress of the Brazilian Geophysical Society, Salvador, p 6

Chapman S, Bartels J (1940) Geomagnetism. Oxford University Press, Oxford

Chapman DS, Pollack HN (1975) Global heat flow: a new look. Earth Planet Sci Lett 28:23–32

Cheng P (1978) Heat transfer in geothermal systems. Adv Heat Transf 14:1–105

Cheng P, Lau KH (1974) Steady state free convection in an unconfined geothermal reservoir. J Geophys Res 79:4425–4431

Combarnous MA, Bories SA (1975) Hydrothermal convection in saturated porous media. Adv Hydroscience 10:231–307

Cull JP (1982) An appraisal of Australian heat flow data. BMR J Aust Geol Geophys 7:11–21

Cull JP, Denham D (1979) Regional variations in Australian heat flow. BMR J Aust Geol Geophys 4:1–13

Drummond SE, Ohmoto H (1985) Chemical evolution and mineral deposition in boiling hydrothermal systems. Econ Geol 82:1–26

Elder J (1981) Geothermal systems. Academic, London

Embley RW, Chadwick W, Perfit MR, Baker ET (1991) Geology of the northern cleft segment, Juan de Fuca Ridge: recent lava flows, sea-floor spreading and the formation of megaplumes. Geology 19:771–775

Everett JD (1883) Rep Brit Assoc for 1882. pp 72–90

Fisher AT (1998) Permeability within basaltic oceanic crust. Rev Geophysics 36(2):143–182

Garg SK, Kassoy DR (1981) Convective heat and mass transfer in hydrothermal systems. In: Rybach L, Muffler LJP (Eds) Geothermal systems: principles and case histories. Wiley, New York, pp 37–76

German CR, Briem J, Chin C, Danielsen M, Holland S, James R, Jónsdóttir A, Ludford E, Moser C, Olafson J, Palmer MR, Rudinicki MD (1994) Hydrothermal activity on the Reykjanes Ridge: the Steinahóll Vent-field at 63°06′N. Earth Planet Sci Lett 121:647–654

Giambalvo ER, Fisher AT, Martin JT, Darty L, Lowell RP (2000) Origin of elevated sediment permeability in a hydrothermal seepage zone, eastern flank of the Juan de Fuca Ridge, and implications for transport of fluid and heat. J Geophys Res 105:913–928

Goyal KP, Kassoy DR (1977) A fault-zone controlled model of the Mesa anomaly. In: Proceedings of the third workshop geothermal reservoir engineering, Stanford University, Stanford, pp 209–213

Gray WG, Oneill K, Pinder GF (1976) Simulation of heat transport in fractured, single-phase geothermal reservoirs. Summaries second workshop geothermal reservoir engineering. Stanford University, Stanford, pp 222–228

Hamilton EL (1976) Variations of density and porosity with depth in deep-sea sediments. J Sediment Petrol 46(2):280–300

Hamza VM, Muñoz M (1996) Heat flow map of South America. Geothermics 25(6):599–646

Hamza VM, Verma RK (1969) Relationship of heat flow with the age of basement rocks. Bull Volcan 33:123–152

Hamza VM, Soares FJS, Gomes AJL, Terceros ZD (2005) Numerical and Functional representations of Regional heat flow in South America. Phys Earth Planet Inter 152:223–256

Haymon RM, Fornari DJ, Edwards MH, Carbotte S, Wright D, Macdonald KC (1991) Hydrothermal vent distribution along the east Pacific Rise crest (9°09′–54′N) and its relationship to magmatic and tectonic processes on fast-spreading mid-ocean ridges. Earth Planet Sci Lett 104:513–534

Hofmeister AM, Criss RE (2005) Earth's heat flux revised and linked to chemistry. Tectonophysics 395:159–177

Hofmeister AM, Criss RE (2006) Comment on "Estimates of heat flow from Cenozoic sea floor using global depth and age data", by M. Wei and D. Sandwell. Tectonophysics 428:95–100

Holst PH, Aziz K (1972) A theoretical and experimental study of natural convection in a confined porous medium. Can J Chem Eng 50:232–241

Horai K, Simmons G (1969) Spherical harmonic analysis of terrestrial heat flow. Earth Planet Sci Lett 6:386–394

Jessop AM, Hobart MA, Sclater JG (1976) The world heat flow data collection—1975, Geothermal Series, vol 20. Earth Physics Branch, Energetic Mines and Resources, Ottawa

Jones EJW (1999) Marine geophysics. Wiley, New York pp 1–466

Lee WHK (1963) Heat flow data analysis. Rev Geophys 1:449–479
Lee WHK, McDonald GJF (1963) The global variation of terrestrial heat flow. J Geophys Res 68:6481–6492
Lee WHK, Uyeda S (1965) Review of heat flow data. In: Lee WHK (Eds) Terrestrial heat flow. Geophysical monograph series 8. AGU, Washington, pp 87–100
Lister CRB (1972) On the thermal balance of a mid-ocean ridge. Geophys J R Astron Soc 26:515–535
Lowell RP, Van Capellan P, Germanovich LN (1993) Silica precipitation in fractures and the evolution of permeability in hydrothermal upflow zones. Science 260:192–194
Lubimova EA, Von Herzen RP, Udintsev GB (1965) On heat transfer through the ocean floor. In terrestrial heat flow. In: Lee WHK (ed) Geophysical monograph series, vol 8. AGU, Washington, pp 78–86
Lupton JE, Baker ET, Mottl MJ, Sansone FJ, Wheat CG, Resing JA, Massoth GJ, Measures CI, Feely RA (1993) Chemical and physical diversity of hydrothermal plumes along the East Pacific Rise, 8°45′–11°50′N. Geophys Res Lett 20:2913–2916
McKenzie DP (1967) Some remarks on heat flow and gravity anomalies. J Geophys Res 72:6261–6273
Meyer C, Hemley J (1967) Wall Rock Alteration. In: Barnes HL (ed) Geochemistry of hydrothermal ore deposits. Holt, Rinehart and Winston, pp 166–235
Murton BJ, Klinkhammer G, Becker K, Briais A, Edge D, Hayward N, Millard N, Mitchell I, Rouse I, Rudnicki M, Sayanagi K, Sloan H, Parson L (1994) Direct evidence for the distribution and occurrence of hydrothermal activity between 27° and 30°N on the Mid-Atlantic Ridge. Earth Planet Sci Lett 125:119–128
Pollack HN, Hurter SJ, Johnson JR (1993) Heat flow from the earth's interior: analysis of the global data set. Rev Geophys 31:267–280
Polyak BG, Smirnov YA (1968) Relationship between terrestrial heat flow and tectonics of continents. Geotectonics 4:205–213 (Eng Transl)
Ponte Neto CF, Hamza VM (2004) Estimation of errors in spherical harmonic representation of global heat flow. In: Proceedings of the regional symposium of the Brazilian Geophysical Society, São Paulo, p 6
Pratts M (1966) The effect of horizontal fluid flow on thermally induced convection currents in porous mediums. J Geophys Res 71:4835–4838
Ribando RJ, Torrance KE (1976) Natural convection in a porous medium: effects of confinement, variable permeability and thermal boundary conditions. J Heat Transfer 98:42–48
Sclater JG, Jaupart C, Galson D (1980) The heat flow through oceanic and continental crust and heat loss of the Earth. Rev Geophys 18:269–311
Snelgrove SH, Forster CB (1996) Impact of seafloor sediment permeability and thickness on off-axis hydrothermal circulation: juan de Fuca ridge eastern flank. J Geophys Res 101:2915–2925
Stein C, Stein S (1992) A model for the global variation in oceanic depth and heat flow with lithospheric age. Nature 359:123–129
Turcotte DL, Schubert G (1982) Geodynamics application of continuum physics to geological problems. Wiley, New York, pp 1–450
Von Herzen R, Davis EE, Fisher AT, Stein CA, Pollack HN (2005) Comments on "Earth's heat flux revised and linked to chemistry" by A.M. Hoffmeister and R.E. Criss. Tectonophysics 409:193–198
Wei M, Sandwell D (2006) Estimates of heat flow from Cenozoic seafloor using global depth and age data. Tectonophysics 417:325–335
Wessel P, Smith WHF (1998) New, improved version of Generic Mapping Tools released. EOS Trans Am Geophys Union 79(47):579
Williams DL, Von Herzen RP, Sclater JG, Anderson RN (1974) The Galapagos spreading center: lithospheric cooling and hydrothermal circulation. Geophys J R Astron Soc 38:587–608